Supporting Information for Plasmonic Heating-Assisted Laser-Induced Crystallization from a $NaClO_3$ Unsaturated Mother Solution

Hiromasa Niinomi[†,‡,*], Teruki Sugiyama[§], Miho Tagawa[//], Mihoko Maruyama[†], Toru Ujihara[//], Takashige Omatsu[‡] and Yusuke Mori[†]

[†]Department of Electrical, Electronic and Information Engineering, Osaka University, Suita, Osaka, 565-0871, Japan

[‡]Molecular Chirality Research Center (MCRC), Graduate School of Advanced Integration Science, Chiba University, Chiba, Chiba, 263-0022, Japan

[§]Department of Applied Chemistry and Institute of Molecular Science, National Chiao Tung University, Hsinchu, 30010, Taiwan

[//] Institute of Materials and Systems for Sustainability (IMaSS), Nagoya University, Nagoya, Aichi, 464-8603, Japan

S1. Polymorphism in $NaClO_3$ crystallization from an aqueous solution

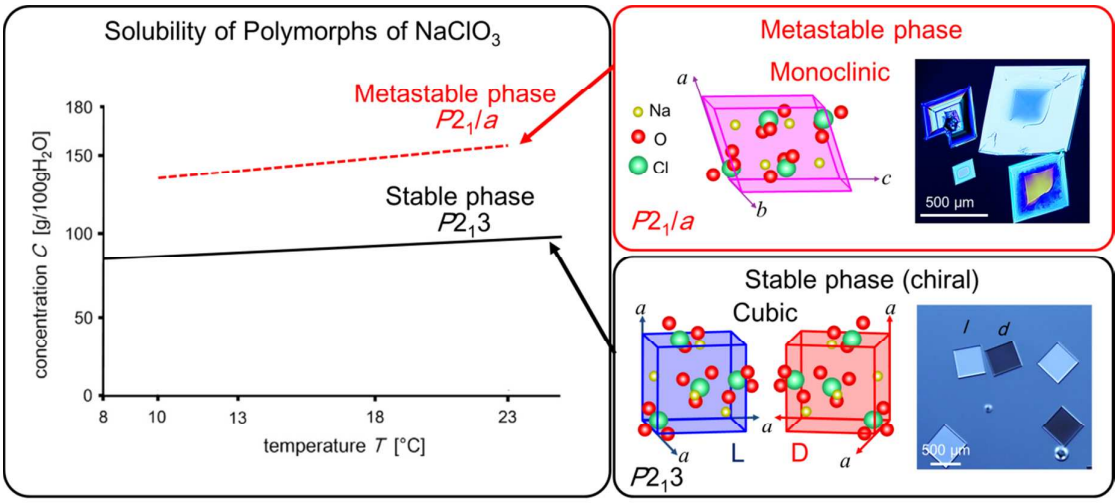

Figure S1. Polymorphism in $NaClO_3$ crystallization from an aqueous solution. $NaClO_3$ crystallizes in two kinds of polymorphic forms: (1) cubic phase with $P2_13$ symmetry as the stable phase; (2) monoclinic phase with $P2_1/a$ symmetry as a metastable phase.[31] The graph depicted in the left side indicates the solubility curve of the polymorphs in the temperature range from 8 °C to 25 °C.[32] The red broken line and the black solid line indicate the solubility of the monoclinic metastable phase and cubic stable phase, respectively. The schematic depicted in the right side shows the crystal structure of the unit cell of the each polymorph. The micrographs listed in the right of the crystal structure shows polarized-light micrographs.

S2. Optical Setup for Laser-Trapping system

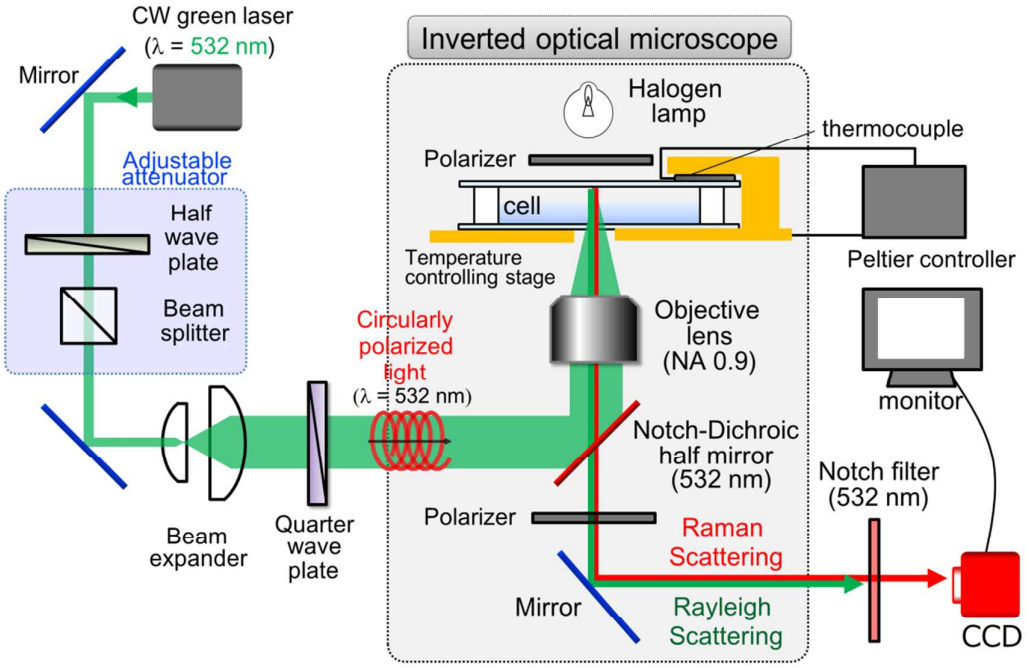

Figure S2. A schematic illustration representing the laser-trapping system for laser-induced nucleation experiment using circularly polarized light.[26]

S3. Intense Raman scattering at the periphery of the focal spot.

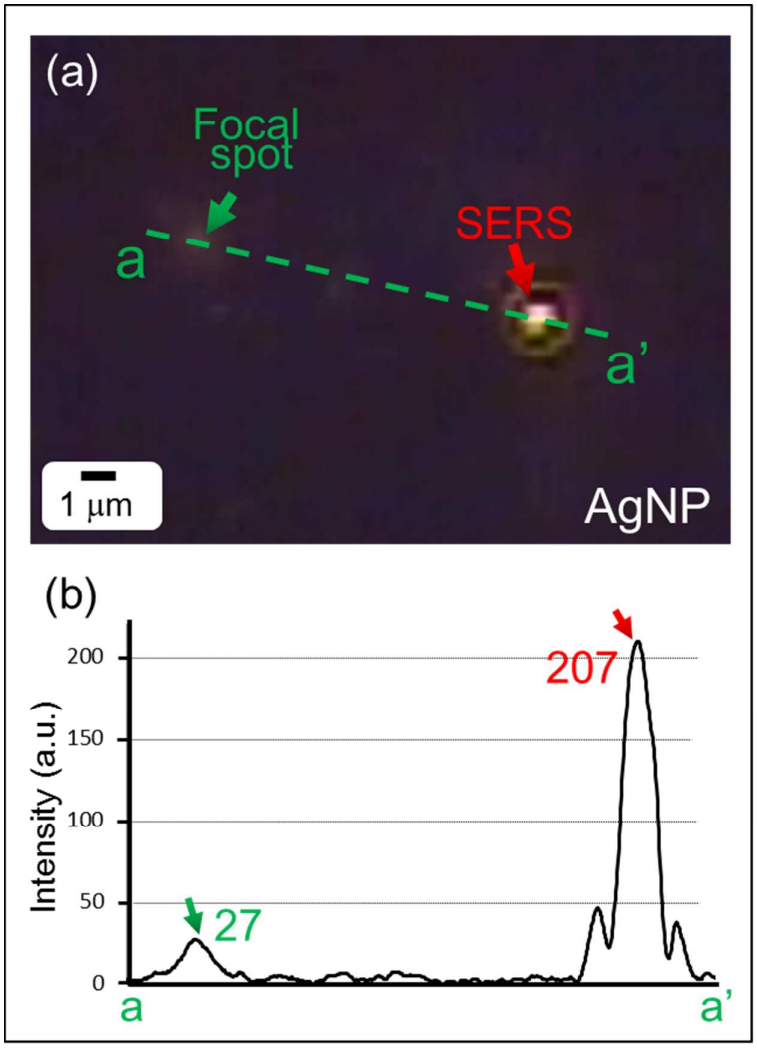

Figure S3. Comparison of intensities between Raman scattering from the focal spot and surface-enhanced Raman scattering from the periphery of the focal spot. (a) A micrograph showing Raman scattering during the crystallization experiment. The green arrow indicates the position of the focal spot and the red arrow indicates surface enhanced Raman scattering. The green dotted line corresponds to the horizontal axis in (b). (b) An intensity distribution profile for the green dotted line a-a'. According to conventional Raman scattering, the maximum intensity should be at the focal spot. However, Figure 2 shows that the maximum was at periphery of the focal spot rather than at the focal spot. Moreover, the intensity of the observed maximum was 207 in 256 gradation whereas that of the focal spot was 27. The observed maximum intensity largely exceeds the intensity of the Raman scattering from the focal pot. This large intensity can be explained by surface-enhanced Raman scattering (SERS).

S4. Comparison of spatial intensity distribution of Raman scattering between the case of SiO_2NP and the case of AgNP

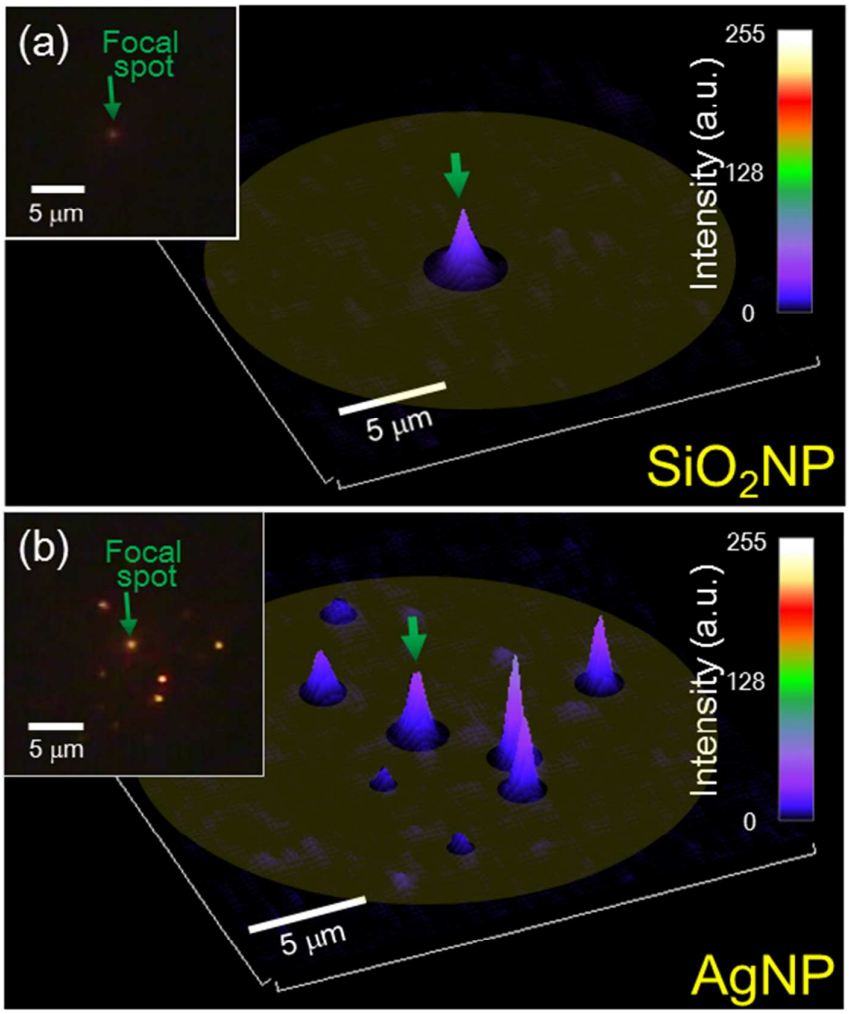

Figure S4. Comparison of spatial intensity distributions between the case that non-metallic SiO_2NPs was used instead of AgNPs and the case that AgNPs was used. (a) The spatial intensity distribution in the case of SiO_2NPs. The inset is the corresponding micrograph. The green arrow indicates the position of the focal spot. The intensity of Raman scattering was expressed by 256 gradation. The area shadowed by yellow is region in which no Raman intensity was detectable in this case. (b) The spatial intensity distribution in the case of AgNPs. Intensities stronger than the intensity at the focal spot can be observed even in the region where no Raman intensity was detectable in the case of SiO_2NPs.

S5. A micrograph showing a salt-induced aggregation of AgNPs

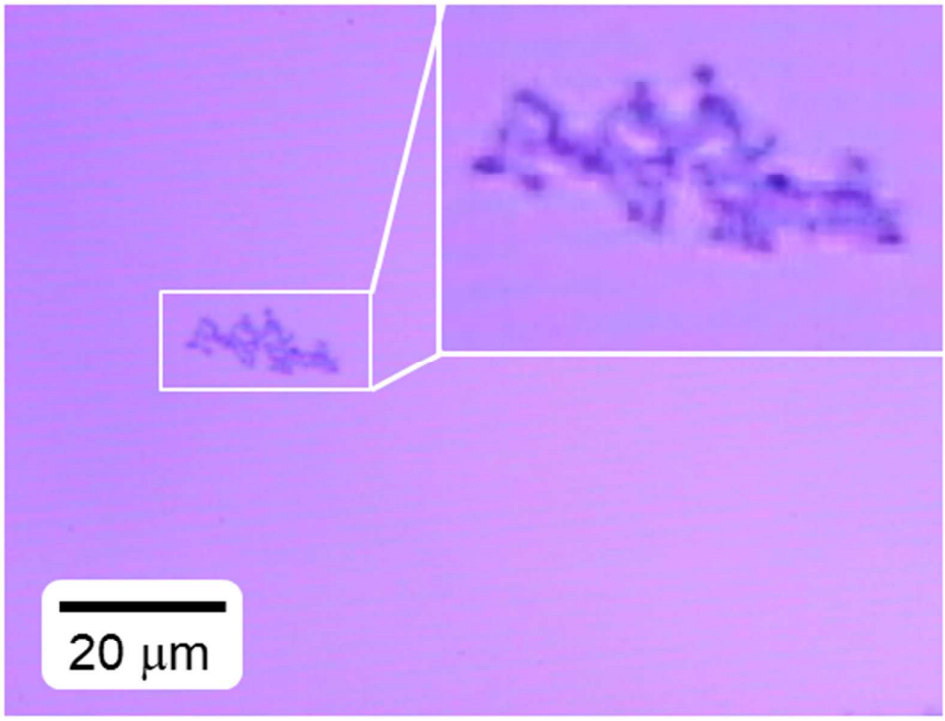

Figure S5. A micrograph showing aggregates of AgNPs floated on air/solution interface.

S6. Time-lapse spatial intensity distribution of Raman scattering from $NaClO_3$ aqueous solution without AgNPs

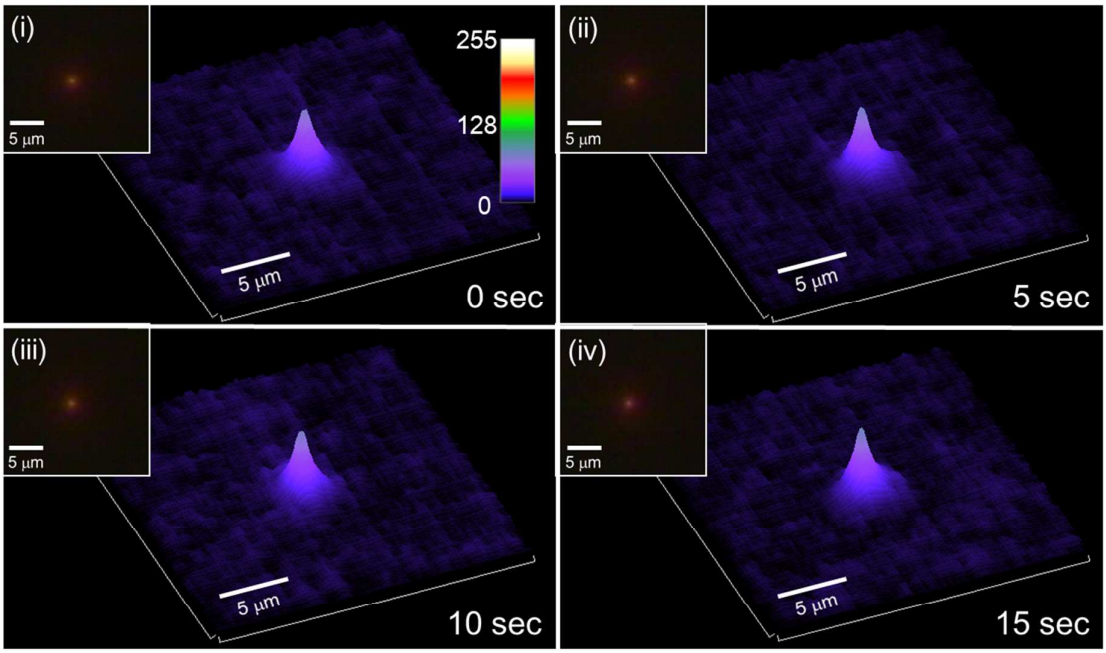

Figure S6. Time-lapse spatial intensity distribution of Raman scattering from $NaClO_3$ aqueous solution without AgNPs. No Raman scattering was detectable excepted for the focal spot in contrast to the case of presence of AgNPs.

S7. Movie of In-situ simultaneous observation of Raman scattering and polarized light image during the laser-induced crystallization.

Figure S7. A captured micrograph of the in-situ simultaneous observation of Raman scattering and polarized light image of $NaClO_3$ crystallization process induced by circularly polarized light laser trapping of Ag nanoparticles at the air/solution interface.

S8. Bubble formation induced by plasmonic heating from an optically-trapped AgNPs at liquid paraffin/$NaClO_3$ aqueous solution containing AgNPs

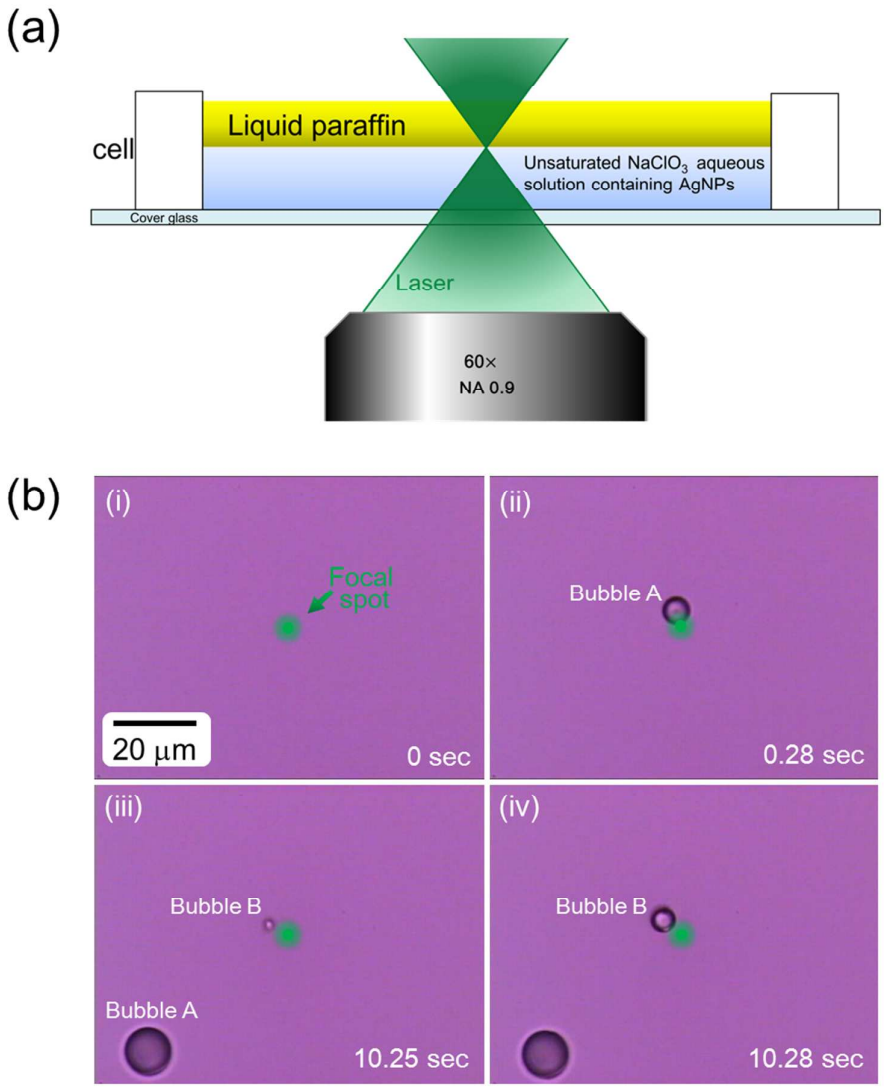

Figure S8. Bubble formation induced by the irradiation of tightly-focused laser to liquid paraffin/solution interface. (a) Schematic illustration describing the experimental setup to confirm the solvent evaporation by plasmonic heating. By covering the solution containing AgNPs using liquid paraffin, whose specific gravity is smaller than that of the solution, vaporized solvent was confined in the liquid paraffin/solution interface. (b) Time-lapse micrographs showing the bubble formation from the focal spot. The green spot indicates the focal spot of the laser. Bubbles which are generated by the evaporation of solvent appeared intensively from the focal spot, supporting that plasmonic heating is sufficient to solvent evaporation. Additonally, crystal formation was never observed under this experiment, indicating the crystallization requires solvent evaporation.

S9. Conversion of the electrical field intensity analyzed by FDTD calculation to power as heat source in FDM simulation.

The power of the light, I_{FDTD}, was calculated using the electrical field intensity analyzed by FDTD calculation, E_0, by following equation;

$$I_{FDTD} = \frac{\pi}{16}\varepsilon_0 c w_1 w_2 |E_0|^2 \quad \text{(S9-1)}$$

where ε_0 is the electrical permittivity of the vacuum, w_1 and w_2 are the widths of the Gaussian distribution of the light in each coordination. Since the electrical field intensity of the input light source was standardized as 1 [V/m] in FDTD analysis, it is necessary to multiply a coefficient which converts the input value to an actual value of electrical field intensity by $|E_0|^2$ in order to calculate the power as heat source on FDM heat transfer simulation. The coefficient, α, is defined as;

$$\alpha = \frac{16 I_{exp}}{\pi \varepsilon_0 c w_1 w_2} \quad \text{(S9-2)}$$

where I_{exp} is experimentally measured value of the intensity of the light source. To multiply α by $|E_0|^2$ allows us to calculate the power as heat source on FDM heat transfer simulation.

S10. Movie of In-situ simultaneous observation of metastable phase crystallization synchronized with the optical trapping of an aggregate of AgNPs.

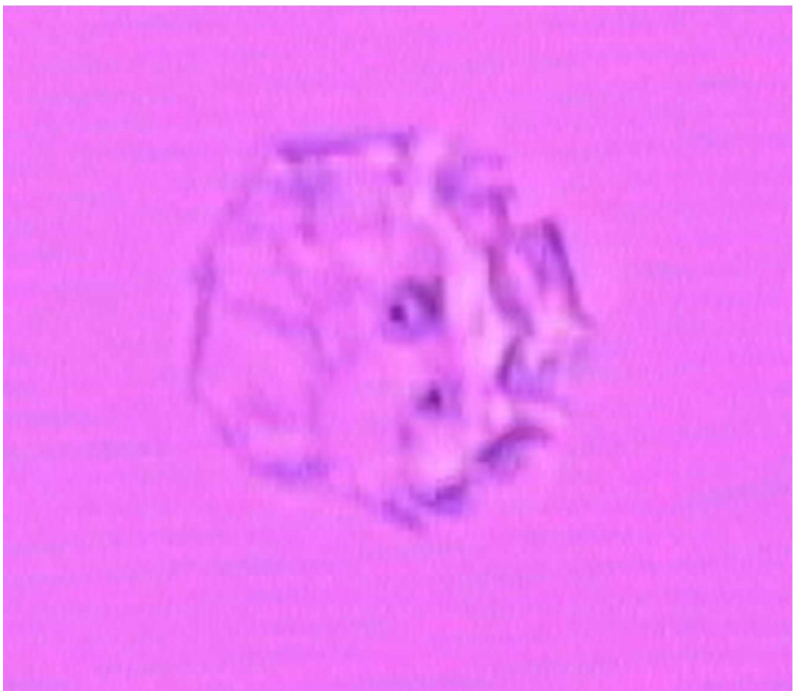

Figure S9. A captured micrograph of the in-situ polarized microscopic observation of $NaClO_3$ crystallization process induced from an optically-trapped aggregates of AgNPs.